Solar Energy
and Sustainable Development
Refereed, biannual scientific journal issued by
The Libyan Center for Solar Energy Research and Studies

DFT Analysis of Structural, Elastic and Optoelectronic Enhancements in $LiGeCl_3$ Under Pressure for Photovoltaic Applications

Mohammed Miri [1*], Younes Ziat [2], Hamza Belkhanchi [3], Abdellah Bouzaid [4], Youssef Jouad [5], Youssef Ait El Kadi [6]

[1, 2, 3, 4, 5] Engineering and Applied Physics Laboratory (EAPL), Superior School of Technology, Sultan Moulay Slimane University, Beni Mellal, Morocco

[1, 2, 3, 4, 5] The Moroccan Association of Sciences and Techniques for Sustainable Development (MASTSD), Beni Mellal, Morocco

[6] Engineering Sciences and Energy Management Laboratory, Higher School of Technology, Ibn Zohr University, Agadir, Morocco

E-*mail:* [1]miri.estbm@gmail.com

SPECIAL ISSUE ON.

The 1St International Conference on Sciences and Techniques for Renewable Energy and the Environment. (STR2E 2025) May 6-8, 2025 at FST-Al Hoceima-Morocco.

KEYWORDS

Absorption; Optical properties; semiconductor; perovskite.

ABSTRACT

This study focuses on the crystalline lithium-based perovskite material, $LiGeCl_3$, with a view to improving its structural, elastic, electronic and optical properties by exploiting the effect of hydrostatic pressure. Combining density of states (DOS and PDOS) analysis with DFT and GGA approximation results, it is shown that the application of pressure reduces the lattice parameter, enhancing self-cohesion and stabilising the atomic structure. At ambient pressure, $LiGeCl_3$ exhibits semiconducting properties with a direct band gap, dominated by the p-orbitals of Cl atoms in the valence band and Ge in the conduction band. Under increasing pressure (0 to 6 GPa), the band gap is progressively reduced until it disappears at 6 GPa, leading to an electronic transition from a semiconducting to a metallic state.

This transition results from the compression of the crystal lattice, which intensifies orbital interactions and causes the valence and conduction bands to overlap. In addition, pressure significantly enhances the optoelectronic properties of $LiGeCl_3$, including absorption in the visible spectrum, spectral reflectivity and refractive index, making the material more suitable for photovoltaic applications. These results highlight the potential of $LiGeCl_3$ in engineering advanced materials for semiconductor and optoelectronic devices, while demonstrating the crucial role of hydrostatic pressure as a tool for modulating material properties.

*Corresponding author.

DOI: https://doi.org/10.51646/jsesd.v14iSTR2E.1181

تحليل DFT للتحسينات الهيكلية والمرنة والبصرية الإلكترونية في $LiGeCl_3$ تحت الضغط لتطبيقات الطاقة الكهروضوئية

محمد ميري، يونس زيات، حمزة بلخنشي، عبد الله بوزايد، يوسف جواد، يوسف ايت القاضي

ملخص: تركز هذه الدراسة على مادة بيروفسكايت الليثيوم البلورية القائمة على الليثيوم، $LiGeCl_3$، بهدف تحسين خصائصها الهيكلية والمرنة والإلكترونية والبصرية من خلال استغلال تأثير الضغط الهيدروستاتيكي. من خلال الجمع بين تحليل كثافة الحالات (DOS وPDOS) مع نتائج تحليل DFT وتقريب GGA، يظهر أن تطبيق الضغط يقلل من معامل الشبكة، مما يعزز التماسك الذاتي ويثبت البنية الذرية. عند الضغط المحيط، يُظهر $LiGeCl_3$ خصائص شبه موصلة مع فجوة نطاق مباشرة، تهيمن عليها المدارات p لذرات Cl في نطاق التكافؤ وGe في نطاق التوصيل. تحت ضغط متزايد (من 0 إلى 6 جيجا باسكال)، تتقلص فجوة النطاق تدريجيًا حتى تختفي عند 6 جيجا باسكال، مما يؤدي إلى انتقال إلكتروني من حالة شبه موصلة إلى حالة معدنية. وينتج هذا الانتقال من انضغاط الشبكة البلورية التي تكثف التفاعلات المدارية وتتسبب في تداخل نطاقات التكافؤ والتوصيل. وبالإضافة إلى ذلك، يعزز الضغط بشكل كبير من الخصائص الإلكترونية الضوئية لـ $LiGeCl_3$، بما في ذلك الامتصاص في الطيف المرئي والانعكاسية الطيفية ومعامل الانكسار، ما يجعل المادة أكثر ملاءمة للتطبيقات الكهروضوئية. وتسلط هذه النتائج الضوء على إمكانات $LiGeCl_3$ في هندسة المواد المتقدمة لأشباه الموصلات والأجهزة الإلكترونية الضوئية، مع إظهار الدور الحاسم للضغط الهيدروستاتيكي كأداة لتعديل خصائص المواد.

الكلمات المفتاحية: الامتصاص؛ الخواص البصرية؛ أشباه الموصلات؛ البيروفسكايت.

1. INTRODUCTION

Today's environmental challenges, such as dependence on unsustainable energy sources and their negative impact on the environment, call for innovative, ecosystem-friendly solutions [1]. Energy transition has become a global priority, with growing interest in the development and adoption of renewable energies, notably photovoltaics and wind power. These technologies offer a unique opportunity to produce clean energy while significantly reducing greenhouse gas emissions, by harnessing abundant natural resources such as solar cells and wind [2, 3, 4].

In this context, solar cells occupy a central position as key solutions for sustainable energy [5]. They have been the focus of intensive research aimed at fully exploiting their potential for converting solar energy into electricity. This work has focused on analyzing the intrinsic properties of photovoltaic materials, in particular their photonic and photoluminescent characteristics, which play a crucial role in improving their efficiency and durability [6]. This in-depth exploration has also uncovered other remarkable properties of the materials used, including their ability to be integrated into advanced devices such as lasers, radiation detectors or thermoelectric systems [7, 8, 9].

Among these materials, perovskites have attracted particular interest thanks to their unique chemical structure and great versatility [10, 11, 12]. Their ABX_3 structure (where "A" and "B" are metal cations and "X" is an anion, often a halogen) gives these materials exceptional properties for photovoltaic applications [13]. For example, studies on $CsXCl_3$ perovskites (X = Sn, Pb) have demonstrated a clear relationship between their lattice parameter and their band gap, establishing a direct link between their crystal structure and their electronic properties [14]. These results underline the importance of theoretical modeling in understanding the fundamental behavior of materials.

With this in mind, density functional theory (DFT) has established itself as an essential tool for analyzing the properties of materials, particularly in the field of perovskites [15, 16].

Beyond the study of intrinsic characteristics, the application of hydrostatic pressure has been identified as a promising lever for tuning and optimizing electronic, optical and mechanical properties. Work on $AGeF_3$ compounds (A = K, Rb) has revealed that pressure can significantly enhance atomic interactions, thereby modifying elastic constants, band gap and other key properties [10, 17, 18, 19]. These results demonstrate that by manipulating external conditions, such as pressure, materials can be optimized to meet the requirements of advanced technological applications [20, 21, 22].

During this time, the $LiGeCl_3$ production is a study and comparison with other theoretical analytical elements and experiments. It does not work because there is no experimental solution available regarding the crystalline structure and the proprietary electronics of $LiGeCl_3$. This signifies the limit of the original approximation and simulation numbers to improve these properties. In the absence of experimental research, we have discovered that the first exploration theory of $LiGeCl_3$ will be visible to future experimental investigations that reveal these results [23, 24]. $LiGeCl_3$ differs from other metal halides in its more gradual and controlled phase transitions under pressure, allowing for finer modulation of optoelectronic properties. Unlike the halide perovskites $CsPbCl_3$ and $RbGeCl_3$, which undergo more abrupt and less stable transitions [25, 26, 27, 28], $LiGeCl_3$ offers greater flexibility and reliability, opening the way for applications in high-pressure environments requiring optimal optical and electronic stability. $LiGeCl_3$ offers precise and stable control of its electronic and optical properties under pressure, unlike more unstable perovskites. Its gradual phase transitions give it better adaptability to extreme environments, ensuring increased durability and reliability for high-pressure applications.

In this context, this study focuses on $LiGeCl_3$ perovskite, a particularly promising material for photovoltaic and optoelectronic technologies [29]. Using density functional theory, we analyze its optoelectronic, mechanical and elastic properties, taking into account the effect of pressure. The application of pressure leads to significant changes in crystal structure, lattice parameters and chemical bonding, resulting in notable improvements in material performance. By exploring these aspects, this research contributes to an in-depth understanding of the relationships between lattice parameters, band gap and mechanical stability under pressure. This knowledge paves the way for optimizing perovskites for next-generation energy and technology applications, responding to the growing need for sustainability and efficiency in renewable energies.

2. CALCULATION METHOD

To study the characteristics of the $LiGeCl_3$ material, density functional theory (DFT) was used, based on the WIEN2k code, known for its precision in modeling crystalline materials [30, 16, 11, 12]. This method is based on linearized full potential augmented waves (FP-LAPW), enabling detailed analysis of electronic, structural and optical properties. To describe exchange and correlation interactions, the generalized gradient approximation (GGA), based on the Perdew-Burke-Ernzerhof (GGA-PBE) formalism, has been applied [31, 32], this approach enables better modeling of electronic interactions by taking into account spatial variations in electron densities, thus improving the accuracy of predictions and making this methodology particularly suitable for the study of crystalline systems such as $LiGeCl_3$. To guarantee adequate

accuracy, the parameter RMTKmax, which corresponds to the product between the radius of the Muffin-Tin sphere and the maximum wave vector, was set to an optimum value after convergence tests. The radii of the Muffin-Tin spheres were adjusted for each atom, taking into account the dimensions of the crystal lattice. A dense k-point grid, based on the Monkhorst-Pack method, was used to sample the Brillouin zone with optimized density, guaranteeing reliable results for total energies and electronic properties. The static calculations for the $LiGeCl_3$ material were performed with a dense mesh of 1000 k-points and energy convergence limit of 10^{-5} Ry to ensure accuracy. The relation $RMT.K_{max} = 7$ was used to optimize the calculation basis and balance accuracy and efficiency. The atomic sphere radii (RMT) for Li, Ge, and Cl atoms are 2.50, 2.50 and 2.32, respectively.

The effect of hydrostatic pressure was simulated by applying uniform stresses to the optimized crystal cell. Calculations were carried out for pressures ranging from 0 GPa to 6 GPa, with regular increments, and at each step, a complete optimization of the geometry enabled the total energy to be minimized and the lattice parameters to be readjusted according to the applied stresses. This approach made it possible to explore variations in electronic, optical and mechanical properties under pressure.

Electronic properties were studied through electronic band structures and densities of states, enabling the evolution of the band gap with pressure to be monitored. Optical properties, such as absorption coefficient, refractive index and complex dielectric function, were calculated taking into account state-dependent electronic transitions. Elastic constants were also determined by applying small strains to the optimized lattice parameters, enabling mechanical stability to be assessed and material stiffness variations to be analyzed under stress.

Thanks to this methodology, it has been possible to provide a comprehensive analysis of the fundamental properties of $LiGeCl_3$, highlighting its optoelectronic and mechanical behavior under various pressure conditions. These results are essential for optimizing the performance of this material in advanced technological applications, notably in photovoltaic and optoelectronic devices.

3. RESULTS AND DISCUSSION

3.1. Structural Properties

The cubic structure of $LiGeCl_3$ belongs to the class of single-halide inorganic perovskites, renowned for their unique crystallographic arrangement and remarkable properties. As illustrated in Figure 1, the crystal structure of $LiGeCl_3$ consists of a unit cell containing five distinct atoms. The geometric configuration and precise arrangement of these atoms play a decisive role in the material's optoelectronic and mechanical properties.

Inorganic perovskites based on metal halides, such as $LiGeCl_3$, are particularly valued for their high symmetry and structural stability. These features make them ideal for theoretical research using advanced computational methods such as density functional theory (DFT), as well as for practical applications in fields such as photovoltaic and optoelectronic devices. The simplicity of the cubic structure provides a solid basis for modeling and predicting material performance under a variety of conditions. In this cubic structure, which belongs to space

group 221 (Pm3m), the Li cation is located in (0, 0, 0), the metal cation Ge in (0.5, 0.5, 0.5), and the Cl anions are arranged in (0.5, 0, 0.5), (0.5, 0.5, 0) and (0, 0.5, 0.5) according to Wyckoff coordinates [33]. The unit cell characterized by lattice parameter of $LiGeCl_3$ is a0= 5.21 Å, these values corresponding to the theoretical values in which a0= 5.19 Å [34]. This perfectly symmetrical and balanced arrangement is essential for maintaining the material's structural and electronic properties.

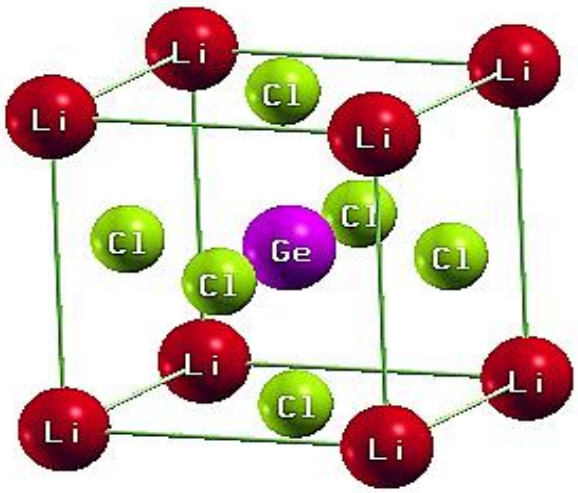

Figure 1: Structure crystalline of $LiGeCl_3$

Detailed understanding of this atomic structure provides a valuable basis for exploring the relationships between structure and material properties, such as mechanical stability, elastic constants and electronic transitions. These fundamental characteristics confirm $LiGeCl_3$'s potential as a key material for many modern technological applications, particularly in the fields of energy and advanced electronics.

To optimize the material's stability and strength, the size of the unit cells was carefully adjusted while taking into account the total energy of the system. This approach has enabled us to determine the optimum structural parameters for stable crystal formation and low energy. The lattice parameter, which determines the dimensions of the unit cell, plays a crucial role in determining the overall properties of the material.

Precise total energy calculations were carried out by systematically varying the size of each unit cell. These variations were used to plot a characteristic energy-volume curve, describing the energy behavior of the crystal as a function of lattice compression or expansion. To analyze these data, the Birch-Murnaghan equation of state was used [35].

$$E = E_0 + \frac{B_0}{B_0'}(V - V_0) - \frac{B_0 V_0}{B_0'(1-B_0')}\left[\left(\frac{V}{V_0}\right)^{1-B_0'} - 1\right] \quad (1)$$

This equation offers a robust theoretical framework for modeling the relationship between energy, volume and pressure in crystalline solids, and is particularly well suited to describing behavior under high pressure or extreme conditions, providing valuable information on the structural stability of materials.

By minimizing the total energy E while optimizing the volume V of the unit cell, the

optimal values of two critical parameters, the mass modulus B and its derivative B′ at zero pressure, have been determined (see Figure 2). These two parameters provide essential information on the mechanical response of the material and are crucial for designing strong, stable structures.

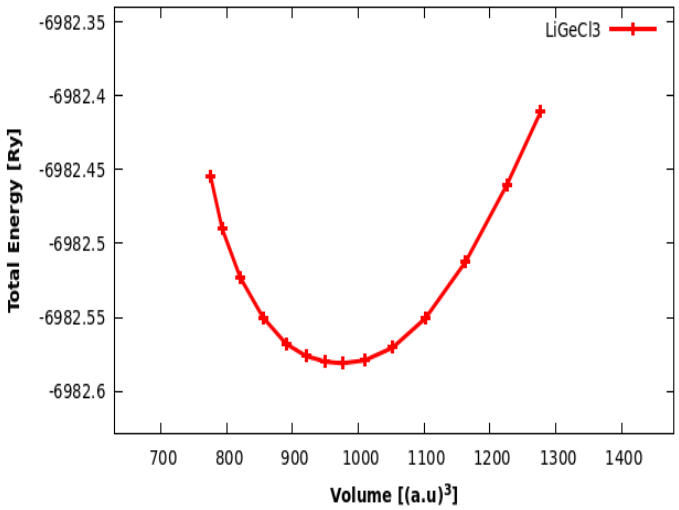

Figure 2 : Variation of total energy as a function of volume for $LiGeCl_3$

The mass modulus B, which measures the material's resistance to compression, is particularly important for applications requiring strength and durability. A high value of B indicates high stiffness. The derivative B′, representing the variation of B under pressure, provides additional information on the material's thermoplastic and elastic properties, such as ductility and crystalline rigidity [36]. Simultaneous optimization of B and B′ improves the overall strength of the material and its ability to resist deformation under stress.

Table 1 summarizes the optimized parameters E, V, B, and B′, providing an overview of the structural performance of $LiGeCl_3$. These results also enable relevant comparisons between different materials and crystal configurations, contributing to a better understanding of structure-property relationships.

Table1: Lattice parameters and gap energy as a function of pressure of $LiGeCl_3$

Lattice Parameter a_0 (Å)		E (Ry)	V (a.u)^3	B (GPa)	(B')
Optimized	Other				
5.21	5.19 [34]	970.77	6982.58	28.97	4.71

The dependence of the cubic lattice constant on pressure was determined using the relationship established by according to the following formulae [37]:

$$P(V) = \frac{B_0}{B_0'}\left[\left(\frac{V_0}{V}\right)^{B_0'} - 1\right] \quad (2)$$

$$a_0 = (V(P))^{1/3} \quad (3)$$

Moreover, the results are summarized in Table 2.

Table 2: Lattice parameter and gap energy versus pressure.

Pressure (GPa)	Parameter a_0 (Å)	Energy Gap Eg (eV)
0	5.21	0.72
2	5.11	0.34
4	5.03	0.12
6	4.97	0.00

Hydrostatic pressure has a significant influence on the structural and electronic properties of materials such as $LiGeCl_3$. As pressure increases from 0 to 6 GPa, there is a steady decrease in the lattice parameters and cell volume, which results in a reduction of interatomic distances. This closer atomic proximity strengthens chemical bonds and enhances the repulsive forces between atoms, leading to greater rigidity and hardness in the crystal structure. These structural changes contribute to an improved mechanical response and increased resistance to crystalline compression under high pressure.

The influence of pressure on the electronic properties of $LiGeCl_3$ is equally notable. At zero pressure, the material exhibits a direct band gap of 0.72 eV, making it suitable for electronic and optoelectronic applications. However, with increasing pressure, the band gap undergoes significant changes. Initially, the band gap widens, reflecting the saturation of compression effects on electronic transitions, as observed in Table 2. Conversely, Table 2 illustrates that under the influence of PBE-GGA functions, the band gap decreases with increasing pressure, a behavior attributed to structural effects. The reduction in lattice constants narrows the atomic distances, intensifies electron-ion interactions, and increases the overlap of atomic orbitals. This leads to a decreased energy separation between the valence and conduction bands, thereby reducing the band gap.

These findings underscore the dual effects of hydrostatic pressure on both structural and electronic properties. While it enhances the material's strength and hardness by intensifying interatomic interactions, it simultaneously modifies electronic transitions, affecting its band gap characteristics. Such insights are crucial for applications requiring materials with stable structural and electronic properties under high-pressure conditions.

3.2. Elastic properties:

The elastic constants of solids represent fundamental parameters that make it possible to describe the mechanical behavior of materials. These constants characterize in particular the way in which a solid reacts to mechanical deformations under the influence of external stresses. In the case of crystals with a cubic structure, such as the studied sample $LiGeCl_3$, there are three independent elastic constants denoted C_{ij}, represented by C_{11} , C_{12} , and C_{44} [38]. These parameters play a fundamental role in assessing the mechanical stability of solids as well as the internal forces acting between their atoms. In addition, they make it possible to establish an accurate relationship between the mechanical properties (such as hardness) and the dynamic properties (such as the propagation of sound waves) of crystals [39]. In order to validate the mechanical stability of materials, the elastic coefficients must satisfy the stability criteria defined by Born [40]:

$$C_{11}+2C_{12} > 0,\ C_{11}-C_{12}>0,\ C_{11}> 0 \text{ and } C_{11}>B > C_{12} \quad (4)$$

The analysis of Table 3 clearly reveals a crystalline stability of $LiGeCl_3$, since the three parameters C_{11}, C_{12} and C_{44} respect the criteria of the limits previously defined. This confirms that the material studied is mechanically stable.

Table 3: Elastic constants of $LiGeCl_3$

Pressure	C_{11}	C_{12}	C_{44}	C_p
0 GPa	46.07	10.68	8.52	2.16
2 GPa	57.44	13.96	9.81	4.15
4 GPa	69.32	16.73	10.54	6.19
6 GPa	78.98	19.20	11.44	7.76

At 0 GPa, the elastic constants and mechanical properties of the material are in good agreement with previous theoretical analyses, thus confirming the validity of the results obtained [34, 23]. When the material is subjected to increasing pressures, ranging from 0 to 6 GPa, a progressive and significant increase in mechanical parameters is observed. This trend indicates a notable improvement in the strength and ductility of the material under compression. When examining the specific elastic constants, it is noted that the constants C_{11} and C_{12} increase at a faster rate than C_{44}. This difference is attributed to the fact that C_{11} ,and C_{12} are mainly influenced by the strengthening of atomic bonds in the longitudinal direction and between crystal planes. Under pressure, these bonds become stiffer, resulting in higher values of these constants. In contrast, C_{44}, which reflects the resistance of the material to shear deformation, shows a more moderate increase. This trend indicates that the flexibility related to shape deformations is less affected by pressure compared to longitudinal and transverse stresses. These disparities in the behavior of elastic constants highlight a complex interplay between the effects of pressure, the overall strength of the material, and its ability to deform without fracture. More specifically, pressure contributes to increasing the material hardness while adjusting its ductility properties, providing a balance between stiffness and flexibility [41]. This correlation is particularly important for applications where robust mechanical properties are required in high-stress environments.

The Cauchy pressure ($C_p=C_{12}-C_{44}$) is a key parameter for assessing the brittleness and ductility of materials, with a positive value indicating ductility and a negative value signaling brittleness [42]. For the perovskite $LiGeCl_3$, Cp remains positive at all pressures studied and increases with pressure, highlighting a progressive improvement in the ductility of the material with increasing pressure. The three moduli — bulk modulus (B), shear modulus (G), and elastic modulus (E) — are essential for evaluating elastic interactions within materials. These parameters help distinguish between ductile materials, which can absorb large amounts of energy before rupture, and brittle materials, which fail abruptly under stress without significant deformation. Such distinctions are critical for understanding how materials behave under mechanical stress, including their capacity to withstand collisions or resist catastrophic failure. These parameters offer a specific classification, adapting to diverse applications: ductile materials for use tolerant of deformations, such as structures, and fragile materials for stable and controlled environments [43]. This analysis provides a comprehensive framework for the design and selection of materials, as well as for industrial applications and technological advancements, in line with Hill's approximations [44, 45, 46].

$$B = \frac{C_{11} + 2C_{12}}{3} \quad (5)$$

$$G = \frac{G_V + G_R}{2} \quad (6)$$

$$E = \frac{9BG}{3B+G} \quad (7)$$

$$\nu = \frac{(3B-2G)}{3(2B+G)} \quad (8)$$

Or

$$G_V = \frac{C_{11} - 2C_{12} + 3C_{44}}{5} \quad (9)$$

$$G_R = \frac{5(C_{11} - C_{12})C_{44}}{4C_{44} + 3(C_{11} - C_{12})} \quad (10)$$

Table 4 shows the significant impact of pressure on the material's elasticity and mechanical strength parameters. As pressure increases, mechanical properties change significantly, reflecting an overall improvement in material performance. The incompressibility modulus (B), which measures the material's resistance to volumetric compression, increases from 22.47 GPa to 39.12 GPa, indicating improved resistance at higher pressures. At the same time, the shear modulus (G), which reflects the material's rigidity to shear-type deformation, increases from 11.47 GPa to 17.00 GPa, reflecting increased rigidity. Furthermore, the modulus of elasticity (E), an indicator of the material's overall capacity for reversible deformation, increased from 29.40 GPa to 44.54 GPa, underlining a significant improvement in its elastic properties.

Based on the moduli B, G and E, two ratios can be determined: Pugh (B/G) [47], and Poisson's ratio (ν), both considered as criteria that describe the proposed mechanical behavior of crystals. B/G and v are identified the brittleness and toughness of materials according to their critical values 1.75, and 0.26 [48], respectively. Whereas brittleness is indicated by a low value, ductility is linked to a high B/G ratio. Roughly 1.75 is the crucial number that divides materials into ductile and brittle categories; that is, (brittle < 1.75 < ductile) [49]. In addition, when Poisson's ratio is greater than 0.26, the material is ductile, and a larger value corresponds to a higher ductility [48]. Analysis of the B/G ratio, which rises from 1.96 to 2.30 at a pressure of 6 GPa, reveals a marked tendency for the material to become more ductile under pressure. This trend is corroborated by the increase in Poisson's ratio (ν), which rises from 0.261 to 0.293. This increase indicates a better ability of the material to resist volumetric deformation, confirming a more ductile behavior as pressure increases.

These results show that the application of pressure simultaneously improves the material's stiffness and ductility, offering an optimum balance between these two properties, essential for applications requiring both mechanical strength and the ability to absorb deformation.

Table 4: The parameters of elastic

Pressure	B	G	E	B/G	v
0	22.47	11.47	29.40	1.96	0.261
2	28.45	13.57	35.12	2.09	0.275

4	34.26	15.35	40.06	2.22	0.286
6	39.12	17.00	44.54	2.30	0.293

3.3. Electronic Properties

The analysis of electronic structures is a fundamental tool for understanding the intrinsic properties of materials, in particular for examining the distribution of energy bands and their evolution under different external factors [50]. This study provides crucial information on the relative position of the top of the valence band (VB), the bottom of the conduction band (CB), and the precise location of the Fermi level. These data not only allow us to characterize the electronic states of a material, but also to differentiate between insulators, semiconductors and conductors according to their band structure. Furthermore, the detailed interpretation of electronic band structures provides information on conduction mechanisms, electron-lattice interaction, and the tailoring of materials' physical properties to technological applications, such as semiconductor devices, sensors, or optoelectronic systems.

In the case of the perovskite $LiGeCl_3$, the electronic band structure was studied under increasing hydrostatic pressures ranging from 0 to 6 GPa, as illustrated in Figure 3. At 0 GPa, the electronic structure at the R symmetry point in the Brillouin zone shows an energy gap of 0.72 eV between CB and VB, confirming that $LiGeCl_3$ is a direct band gap semiconductor. The valence band is well-defined and high, while the conduction band is relatively low, reinforcing its semiconducting behavior at ambient pressure (Figure 3(a)).

With increasing pressure, significant changes in band structure are observed. At 2 GPa and 4 GPa (Figure 3 (a and b)), the CB minimum shifts to lower energies, while the VB maximum remains localized at the R-point. This evolution, while reducing the value of the energy gap to 0.34 eV at 2 GPa and 0.12 eV at 4 GPa, demonstrates that $LiGeCl_3$ retains its direct band gap semiconducting character. However, beyond 4 GPa, the band gap progressively decreases until it becomes 0 ev at 6 GPa, at which point a major electronic transition is observed: the material changes from a semiconducting to a metallic state. This transformation is directly linked to the compression of the crystal lattice and the intensification of interactions between atoms.

Compression under high pressure tightens inter-atomic distances, enhancing interactions between neighboring atomic orbitals. This causes the conduction and valence bands to overlap, removing the energy barrier necessary for electron excitation. As a result, electrons become free to circulate in the crystal, transforming the material's electronic properties from semiconductor to metallic conductor, this phenomenon highlights the crucial impact of pressure on the modulation of electronic properties [51].

Pressure is also emerging as a powerful tool for fine-tuning the optical and electronic properties of crystalline materials. It allows controlled modification of key parameters such as band gap width, density of states and charge carrier mobility. This approach paves the way for the exploration of new states of matter, where phase transitions, changes in crystallographic symmetry, or even novel electronic behaviors can be observed under high pressure. From a practical perspective, the use of pressure in high-performance semiconductor engineering represents a bridge between fundamental research and technological applications.

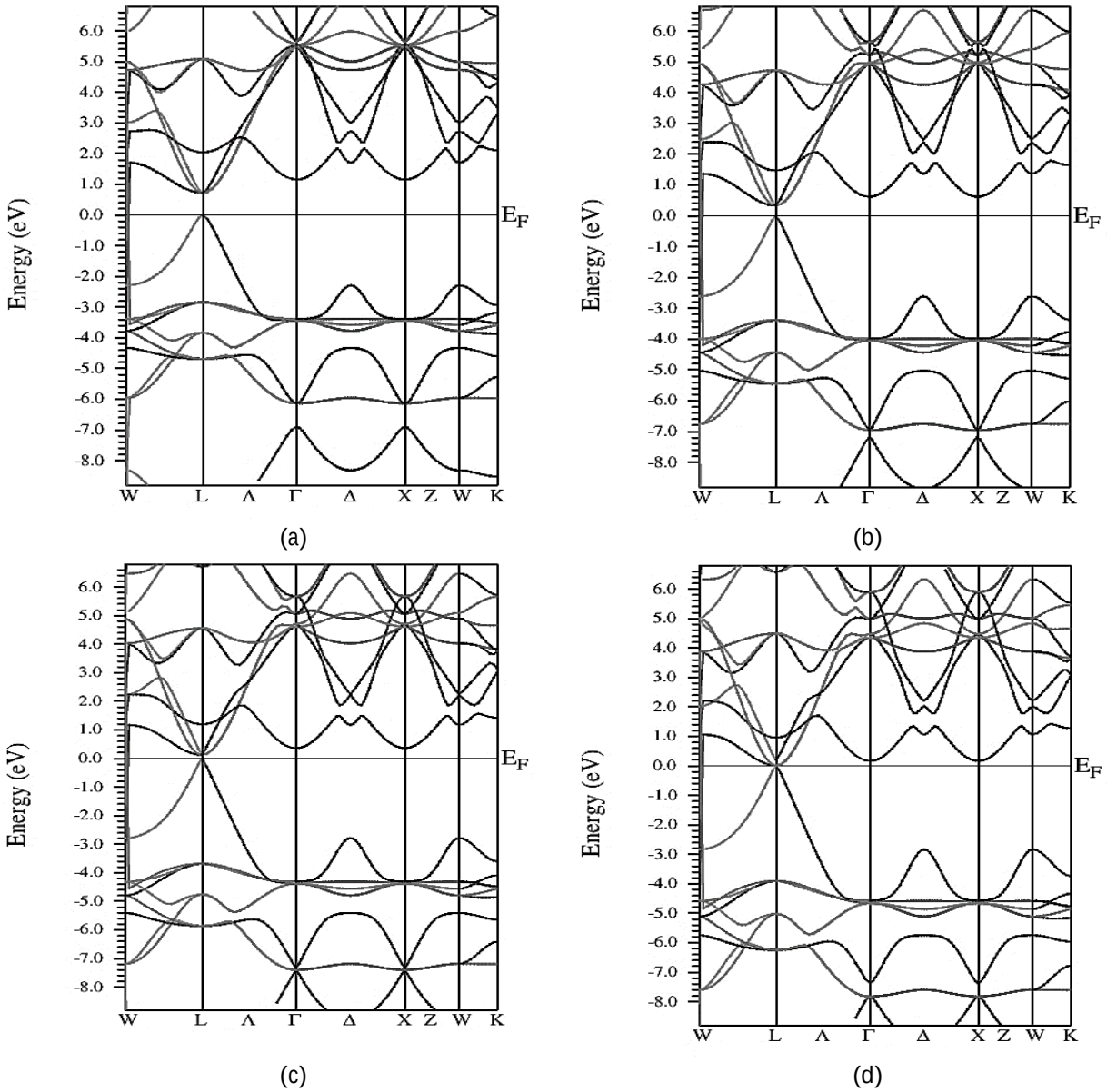

Figure 3 : Band structure at (a) 0, (b) 2, (c) 4 and (d) 6GPa

Figures 4 and 5 illustrate the densities of electronic states (DOS) and projected densities of states (PDOS) for $LiGeCl_3$ perovskite, highlighting the distribution of electronic states within the crystal lattice. These analyses identify the contribution of atoms and orbitals to specific energy levels, offering a detailed understanding of the electronic interactions and fundamental mechanisms of the material. While total density of states (TDOS) gives an overview of the electronic structure, PDOS attributes these contributions to specific atoms such as lithium (Li), germanium (Ge) and chlorine (Cl), and their respective orbitals (s, p and d). This differentiation is crucial to deciphering the atomic and orbital electronic interactions that underlie the fundamental properties of the material.

At zero pressure, the electronic structure of $LiGeCl_3$ reveals a dominance of the p-orbitals of chlorine (Cl) atoms in the valence band (VB), while the conduction band (CB) is mainly influenced by the p-orbitals of germanium (Ge) and to a lesser extent by the s-orbitals of lithium (Li). The main orbital peaks are located as follows: Li s-orbitals at around 3 eV (CB),

Ge p-orbitals at 2.8 eV and 4.5 eV (CB), and Cl p-orbitals at -3.5 eV and -4.5 eV (VB). These observations underline the central role of Ge in the electronic transition properties, as well as the importance of Cl in chemical bonding and balanced electronic interactions within the material. The Fermi level (EF), located just above the peak of the valence band, confirms that $LiGeCl_3$ has a semiconducting nature with a direct band gap. Under pressure, significant changes are observed in the electronic structure. With increasing pressure up to 6 GPa, the p-orbitals of Ge and Cl in the CB approach the Fermi level, reflecting enhanced electronic interaction due to crystal lattice compression. At the same time, the p-orbitals of Cl atoms in the VB shift to lower energies, from -3.5 eV and -4.5 eV to -4 eV and -6.1 eV respectively. These energy shifts reflect an electronic transfer that progressively reduces the band gap width and modifies the material's electronic properties.

Above a critical pressure of 4 GPa, the reduction of interatomic distances intensifies orbital interactions, leading to a significant shift of electronic levels, particularly the p orbitals of Ge and Cl, toward the Fermi level. As pressure increases, the overlap between atomic orbitals becomes more pronounced, increasing the density of states near the Fermi level and facilitating electron transitions to the conduction band. At 6 GPa, this culminates in a semiconductor-to-metal transition, where the band gap completely closes, and the material exhibits metallic conductivity [51]. This behavior, characteristic of materials undergoing significant crystalline compression, results from the enhanced overlap of electronic bands, allowing electrons to flow more freely and transforming $LiGeCl_3$ into a conductive metal.

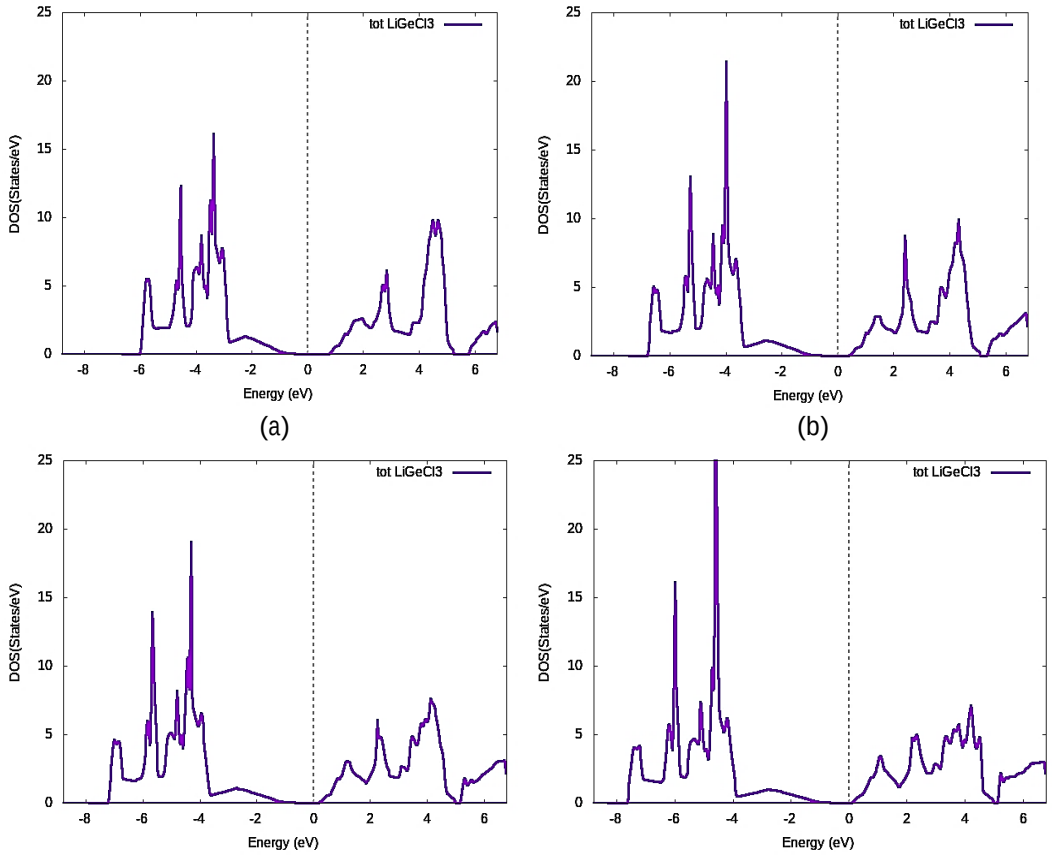

Figure 4: DOS for $LiGeCl_3$ at (a) 0, (b) 2, (c) 4 and (d) 6GPa.

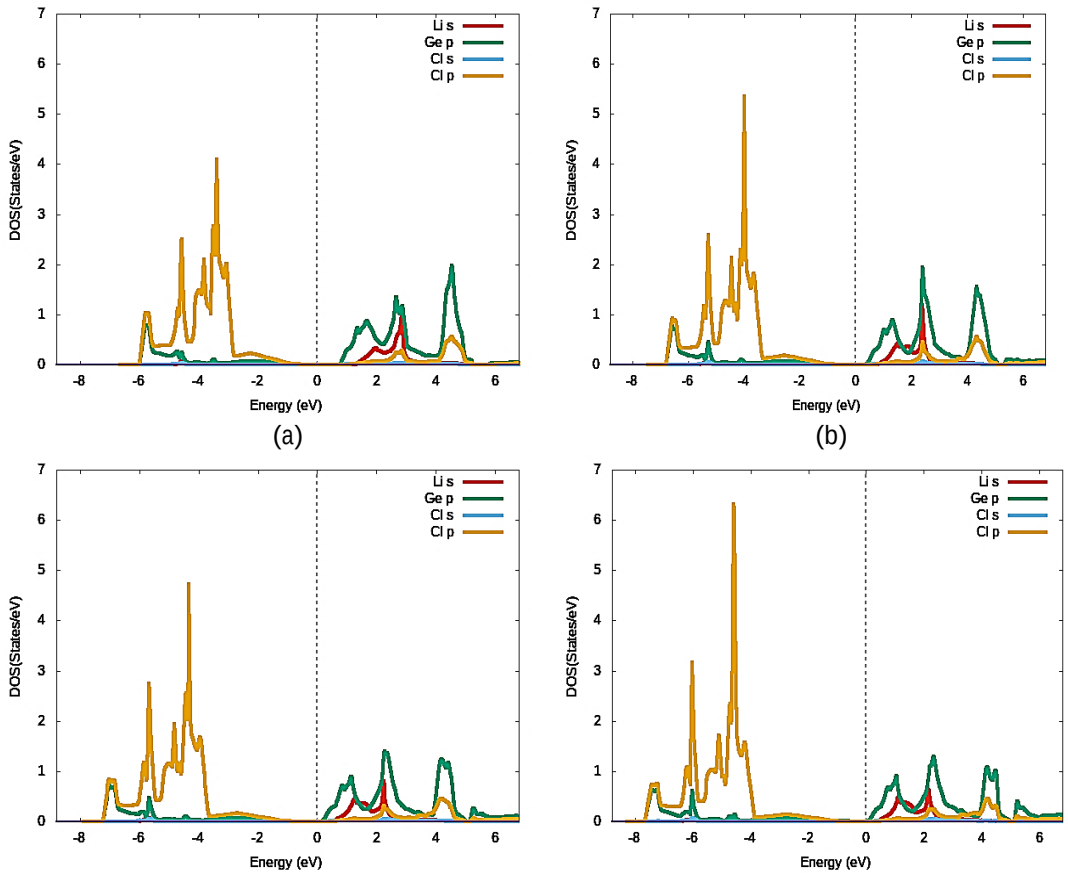

Figure 5: PDOS for $LiGeCl_3$ at (a) 0, (b) 2, (c) 4 and (d) 6GPa.

This pressure-induced phase transition illustrates the crucial role of hydrostatic pressure as a parameter for tuning the electronic and optical properties of materials. The application of pressure not only makes it possible to explore phase transitions and changes in crystallographic symmetry, but also to design materials with controlled electronic properties for advanced applications, notably in semiconductors, optoelectronic devices and pressure-sensitive systems. These results reinforce our understanding of electronic transition phenomena in condensed matter, and pave the way for potential applications in high-performance materials engineering.

3.4. Optical properties

The band gap values of the materials studied, located in the UV and visible ranges, confirm their promising potential for advanced optoelectronic applications. In particular, these materials offer interesting prospects for improving the performance of photovoltaic cells and solar panels, technologies at the heart of renewable energy solutions. The effect of hydrostatic pressure has proved to be a simple and effective method for modulating the electronic structures of materials and, consequently, optimizing their optical properties. In this context, we have examined $LiGeCl_3$ materials under the influence of induced pressure ranging from 0 to 6 GPa. Structural and electronic changes due to this pressure have a significant impact on several key optical properties such as absorption coefficient (α), optical conductivity (σ), reflectance (R) and refractive index (n). These results provide valuable information for the selection and development of new optoelectronic materials. [52, 11].

$$\alpha(\omega) = \sqrt{2}\omega\left[\sqrt{\varepsilon_1^2(\omega) + \varepsilon_2^2(\omega)} - \varepsilon_1(\omega)\right]^{\frac{1}{2}} \quad (11)$$

$$\sigma(\omega) = \frac{\omega}{4\pi}\varepsilon_2(\omega) \quad (12)$$

$$n(\omega) = \frac{1}{\sqrt{2}}\left[\sqrt{\varepsilon_1^2(\omega) + \varepsilon_2^2(\omega)} + \varepsilon_1(\omega)\right]^{\frac{1}{2}} \quad (13)$$

$$R(\omega) = \left|\frac{\sqrt{\epsilon(\omega)} - 1}{\sqrt{\epsilon(\omega)} + 1}\right|^2 \quad (14)$$

In addition, the evolution of optical conductivity and refractive index under pressure testifies to improved light-matter interactions, opening up prospects for applications in advanced photonic systems and integrated optoelectronic devices. These results also underline the importance of materials engineering under stress to tailor optical properties to specific application needs. The data obtained from this study provide valuable information for the design and development of new optoelectronic materials. In particular, the ability of these materials to respond to external pressures while modifying their optical properties represents a significant advance in research into multifunctional materials for next-generation technologies. These results encourage future investigations into the combined effects of pressure and chemical composition in the quest for even higher-performance materials.

The absorption coefficient α(ω) represents a fundamental quantity that quantifies the attenuation of light intensity per unit distance traveled in a material, and is directly related to electronic transitions between energy bands. Detailed analysis of absorption spectra provides essential information on the electronic and optical properties of the material, including its ability to interact with light in different spectral ranges [53]. Absorption spectra calculated for $LiGeCl_3$ under different hydrostatic pressures, shown in Figure 6, reveal significant trends. At ambient pressure (0 GPa), the material remains transparent to photons with energies below around 1.0 eV, corresponding to the band gap width. When the pressure is increased to 2 GPa, 4 GPa and 6 GPa, the absorption thresholds are reduced to 0.8 eV, 0.7 eV and 0.5 eV respectively, indicating a progressive narrowing of the band gap under the effect of pressure. This behavior reflects an increase in the overlap of electronic orbitals and an increased density of states near the Fermi level, favoring electronic transitions at lower energies. Beyond the absorption thresholds, α(ω) values increase progressively with photon energy, reaching maximum peaks of around $138*10^4.cm^{-1}$, $149*10^4.cm^{-1}$, $157*10^4.cm^{-1}$ and $165*10^4.cm^{-1}$ respectively for 0 GPa, 2 GPa, 4 GPa and 6 GPa, around 4 eV. These peaks indicate intense electronic transitions, mainly between valence bands dominated by the p-orbitals of chlorine atoms and conduction bands influenced by the p-orbitals of germanium and s-orbitals of lithium. After these maxima, a decrease in the absorption coefficient is observed, followed by a gradual increase to around 12 eV. This complex optical response is attributed to the diversity of electronic transitions available at high energies, involving electronic states located further away from the fundamental bands. A notable feature of these spectra is the overall shift of absorption peaks towards lower energies as pressure increases, a phenomenon consistent with

the narrowing of the band gap. This shift highlights the effect of hydrostatic pressure on the electronic structure of $LiGeCl_3$, resulting in a significant enhancement of light absorption, particularly in the visible and ultraviolet ranges. Thus, pressure induction appears to be an effective tool for optimizing the optical properties of $LiGeCl_3$, increasing its absorption efficiency in spectral ranges relevant to optoelectronic applications, such as photovoltaic cells and photodetectors. These results confirm the potential of this material in the development of advanced devices, where enhanced absorption in the visible and UV ranges is crucial to maximizing performance.

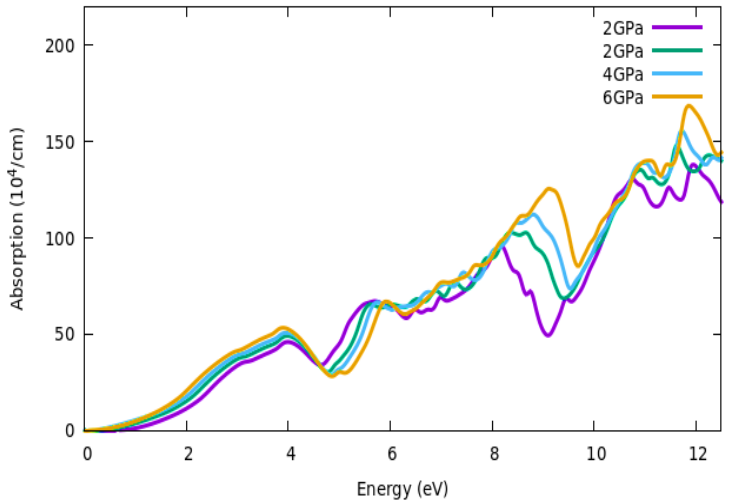

Figure 6: Absorption coefficient versus energy at 0, 2, 4 and 6 GPa for $LiGeCl_3$.

Figure 7 shows the optical conductivity ($\sigma(\omega)$) of $LiGeCl_3$, which reflects the material's ability to carry electric currents upon interaction with an electromagnetic field. Optical conductivity is directly related to interband electronic transitions and is a crucial indicator of the material's optoelectronic properties. In the energy range from 0 to 4 eV, optical conductivity increases steadily. This can be attributed to electronic transitions in the valence bands close to the Fermi level. This region is less influenced by pressure, suggesting that structural modifications due to hydrostatic compression do not significantly affect these low-energy transitions. However, when the photon energy exceeds 4 eV, the optical conductivity shows well-defined peaks that vary significantly in amplitude and position under the effect of pressure. These peaks, mainly located between 4 and 8 eV, are highly sensitive to increasing pressure. At 6 GPa, peak amplitudes are considerably higher than those observed at ambient pressure, indicating a redistribution of electronic states and an increased density of states available for high-energy interband transitions. This increase in the density of electronic states under pressure can be explained by the increased overlap of electronic orbitals in the compressed crystal lattice, leading to enhanced electronic transitions. Above 8 eV, optical conductivity reaches a saturation point, where it remains high but shows more subtle variations. This may indicate that the majority of electronic transitions accessible at high energies are saturated. In particular, the effect of pressure becomes more pronounced in this high energy range, especially at 6 GPa, where a significant increase in optical conductivity is observed. This increase is indicative of the improved optical and electronic behavior induced

by compression. Analysis of low energies (below 6 eV) reveals that the effect of pressure on optical conductivity remains limited. This suggests that the dominant electronic transitions in this range originate from bands relatively unaffected by pressure-induced structural changes. However, at high energies (above 6 eV), pressure-induced changes become significant, indicating a reorganization of the electronic structure and an increase in the density of available high-energy states. In conclusion, hydrostatic pressure proves to be an effective lever for modifying the electronic structure of $LiGeCl_3$, thereby increasing its optical conductivity, particularly in the high energy ranges. This behavior highlights a potential application in optoelectronic devices, where increased conductivity under pressure can be exploited as a performance factor. Enhanced electronic and optical properties under pressure could also open up interesting prospects for applications in extreme environments or devices requiring fast, efficient response at high energies.

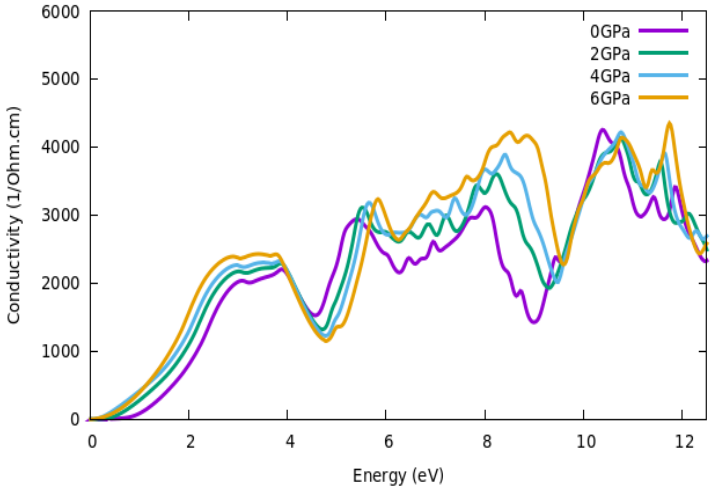

Figure 7: Conductivity versus energy at 0, 2, 4 and 6 GPa for $LiGeCl_3$.

Figure 8 shows the reflectance spectra (R(ω)) of $LiGeCl_3$ subjected to different hydrostatic pressures, highlighting the effect of compression on the optical properties of the material. Reflectance is a key property for characterizing interactions between incident light and the surface of a crystalline material, offering valuable information on optical reflection and absorption processes at the surface [54, 53]. At R(0), reflectance values increase with pressure, rising from 0.165 at 0 GPa to 0.252 at 6 GPa. This increase indicates an improvement in the material's ability to reflect low-energy light, which can be attributed to the change in electron density near the surface under compression. This trend could also reflect an increase in the actual refractive index, often correlated with a densified electronic structure under pressure. Examining the spectra for increasing energies, reflectance increases progressively until around 2.5 eV, where it reaches a maximum. This behavior may be associated with electronic transitions in the lower energy bands, which strongly influence the interaction of incident light with the material's surface and bulk states. At this stage, pressure seems to play a key role in modifying the electronic structure and, consequently, the optical reflection properties. Above 2.5 eV, the spectra show a rapid decline in reflectance up to around 4.5 eV. This decline can be explained by an increase in optical absorption, where more of the incident energy is absorbed by the material, reducing the reflected fraction. This region corresponds to more energetic

electronic transitions, where the photonic interaction penetrates further into the volume of the material, reducing surface reflection. After this drop, reflectance rises again for energies above 4.5 eV. This second rise could be attributed to high-energy interband electronic transitions, where excited electrons interact strongly with incident light, resulting in increased reflection. This increase could also result from a plasmonic effect linked to the increased electron density under pressure. Pressure analysis reveals that reflectance spectra are particularly sensitive to variations in hydrostatic pressure, with a noticeable increase in reflectance values across all the energy ranges studied. This suggests that pressure acts as an effective tool for tuning the optical properties of $LiGeCl_3$, increasing its reflectance, particularly at low frequencies and in certain high energy ranges.

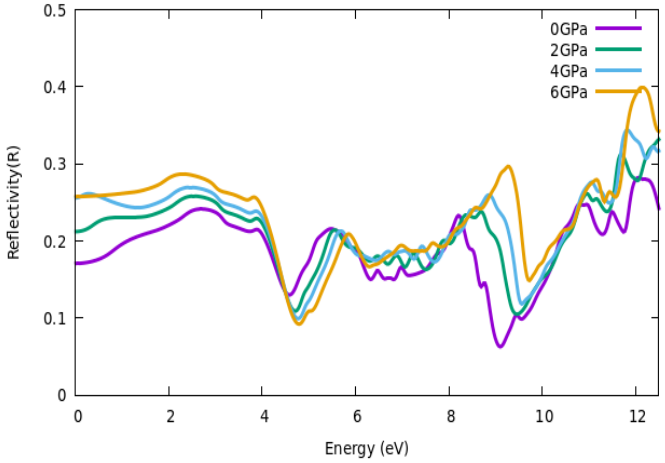

Figure 8: Reflectivity versus energy at 0, 2, 4 and 6GPa for $LiGeCl_3$.

Figure 9 shows spectral variations in refractive index n(ω) of $LiGeCl_3$ under different pressures, offering a detailed insight into how the material interacts with light through its transparency properties. The refractive index is an essential parameter for assessing the propagation speed of light in a material, and provides crucial information on light scattering and diffusion, enabling a better understanding of light-matter interaction mechanisms. Between 0 and 2.5 eV, values of n(ω) are significantly higher under a pressure of 6 GPa, with respective values of 3.21, 3.20, 2.70 and 2.40 at 6 GPa, 4 GPa, 2 GPa and 0 GPa. This increase in refractive index with pressure indicates a densification of the electronic structure under the effect of compression, resulting in a slowing of light propagation in the material. The higher refractive index at higher pressure reflects a pressure-induced increase in electron-induced polarization, which may suggest a better interaction between light and electronic states in this energy range. This decreasing trend in n(ω) with pressure is probably explained by the effect of compression on electronic orbitals. More precisely, increasing pressure causes the crystal lattice to contract, thus modifying electron dynamics and affecting the optical properties of the material, notably its refractive index. High values at 6 GPa may be linked to a greater density of electronic states, facilitating stronger interaction between photons and the material. Above 2.5 eV, the refractive index n(ω) decreases progressively with increasing energy, from relatively high values to a minimum value of around 0.75 at 12 eV. This phenomenon is typical of materials where absorption begins to dominate at higher energies, and the refractive index adjusts accordingly to reflect this transition. The continued decrease in refractive index after

2.5 eV could also be linked to the delocalization of electrons into more energetic states, reducing the material's ability to effectively polarize incident light. This reduction in the 1.5 to 4.3 eV range probably indicates a transition from regimes where light is more strongly scattered to regimes where interactions with excited electrons become less significant.

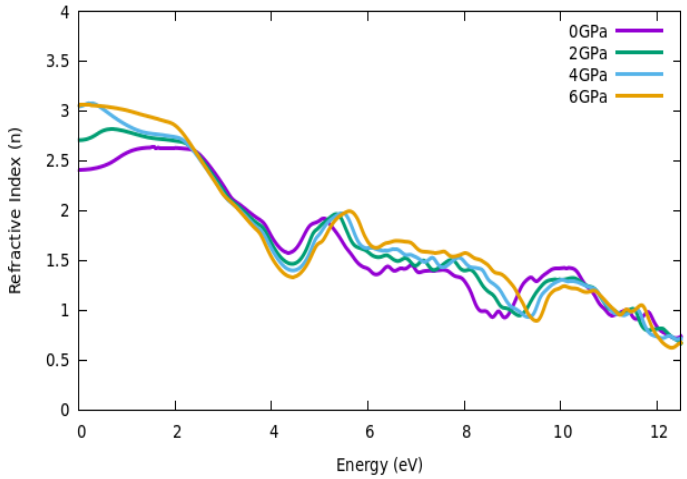

Figure 9: Reflective index versus energy at 0, 2, 4 and 6 GPa for $LiGeCl_3$.

4. CONCLUSION:

The DFT method, implemented in the Wien2k code, has been employed to analyse the physical and optical properties of $LiGeCl_3$ compounds. The results obtained for the equilibrium structure are consistent with previous theoretical studies, confirming the validity of the calculations. The optimization curve was used to evaluate the parameters required to ensure the stability of the systems. Calculations using the GGA reveal that the elastic constants (Cij) of $LiGeCl_3$ meet the criteria for mechanical stability, while the progressive increase in pressure contributes to a reduction in the lattice parameter, leading to a narrowing of the electronic band gap. Analysis of the electronic structures of $LiGeCl_3$ under pressure reveals a notable transition from semiconductor to metal. At ambient pressure (0 GPa), $LiGeCl_3$ has a direct band gap of 0.72 eV, which gradually decreases under pressure (0.34 eV at 2 GPa, 0.12 eV at 4 GPa) before disappearing at 6 GPa, where the material becomes metallic. This transformation, due to the compression of the crystalline lattice and the overlapping of bands, demonstrates the crucial impact of pressure on electronic properties, opening up prospects for the engineering of advanced optoelectronic materials. The study also examined in detail the optical properties of the material under different pressures (from 0 to 6 GPa), focusing on their effects on the electronic structure and optical characteristics of $LiGeCl_3$, including absorption, optical conductivity, reflectance and refractive index. The material's absorption improves in the visible and UV ranges under pressure, with a shift in absorption thresholds towards lower energies and an increase in the absorption coefficient to 6 GPa. These results highlight the increased potential of $LiGeCl_3$ for photovoltaic devices and other optoelectronic applications. Optical conductivity shows a redistribution of electronic states under pressure, with notable changes in conductivity peaks, particularly at high pressures. This indicates a densification of the electronic states, reinforcing the material's conductive properties, particularly at high pressure and high energy. The study revealed a progressive increase in Reflectivity with energy,

modified by pressure. At 6 GPa, the refractive index is significantly higher in the 0-2.5 eV range, indicating better interaction of the material with light. This development is consistent with the compression of the crystal lattice and the increase in electron density. In conclusion, this work shows that hydrostatic pressure is a key parameter for optimizing the electronic and optical properties of $LiGeCl_3$. Under pressure, the material exhibits improved optical characteristics, particularly in the visible and UV ranges, making it particularly promising for modern applications such as photovoltaic cells and light-based optoelectronic devices. The optimization of $LiGeCl_3$ through pressure thus opens up new prospects for the engineering of advanced materials in energy harvesting and other optoelectronic technologies. However, the synthesis and shaping of $LiGeCl_3$ under pressure pose challenges related to its structural stability, with dangers of irreversible structural changes. The challenge of producing uniform materials on a large scale also persists due to the difficulty in ensuring the reproducibility and purity of samples. To integrate $LiGeCl_3$ into operational systems, it is crucial that it is compatible with existing technologies (LEDs, solar panels, sensors), which implies carrying out studies on its deposition and encapsulation. In addition, it is necessary to examine the durability and reliability of the material when subjected to prolonged pressure to prevent any deterioration in its performance.

Author Contributions: Mohammed Miri: Writing – original draft, Visualization, Validation, Investigation, Formal analysis, Data curation, Conceptualization. Younes Ziat: Supervision. Hamza Belkhanchi: Visualization, Validation, Investigation, Formal analysis. Abdellah Bouzaid: Visualization. Youssef Jouad: Visualization. Youssef Ait El Kadi: Visualization. The author also reviewed and edited the manuscript for final approval.

Funding: The authors are warmly grateful to the support of "The Moroccan Association of Sciences and Techniques for Sustainable Development (MASTSD), Beni Mellal, Morocco".

Data Availability Statement: Not applicable.

Acknowledgments: A special thank you to Professor Hanane Reddad from Sultan Moulay Slimane University, Beni Mellal, Morocco, for her technical and scientific support, as well as her full collaboration and discussion during the different steps of the present investigation.

Conflicts of Interest: The authors declare that they have no conflict of interest.

REFERENCE

[1] *D. Shiwen, and F. Zhang. "General applications of density functional theory in photocatalysis." Chinese Journal of Catalysis 61 (2024): 1-36.*

[2] *V. Nitsenko, A. Mardani, J. Streimikis, I. Shkrabak, I. Klopov, O. Novomlynets, & O. Podolska. Crite-ria for evaluation of efficiency of energy transformation based on renewable energy sources. Montenegrin Jour-nal of Economics, 14(4), (2018), 237-247.*

[3] *H. Belkhanchi, Y. Ziat, M. Hammi, C. Laghlimi, A. Moutcine, A. Benyounes, & F. Kzaiber. Nitrogen doped carbon nanotubes grafted TiO2 rutile nanofilms: Promising material for dye sensitized solar cell application. Optik, 229, 166234. (2021), https://doi.org/10.1016/j.ijleo.2020.166234.*

[4] H. Belkhanchi, Y. Ziat, M. Hammi, C. Laghlimi, A. Moutcine, A. Benyounes, & F. Kzaiber. Synthesis of N-CNT/TiO2 composites thin films: surface analysis and optoelectronic properties. E3S Web of Conferences (Vol. 183, p. 05002) (2020), EDP Sciences. https://doi.org/10.1051/e3sconf/202018305002.

[5] F. Yang, Y. Pan, & J. Zhu. Enhanced catalytic activity of noble metal@ borophene/WS2 heterojunction for hydrogen evolution reaction. Applied Surface Science, 680, 161321 (2025).

[6] A. Waqdim, M. Agouri, A. Abbassi, B. Elhadadi, Z. Zidane, S. Taj, M. El Idrissi, Theoretical investigation of the physical properties of cubic perovskite oxides SrXO3 (X= Sc, Ge, Si). Mater. Sci. Semicond. Process. 158, 107340 (2023)., https://doi.org/10.1016/j.mssp.2023.107340.

[7] F.Zhang, Y. Mao, T.J. Park, S.S. Wong, Green synthesis and property characterization of single-crystalline perovskite fluoride nanorods, Adv. Funct.Mater. 18 (1) (2008) 103112..

[8] S. Collavini, S.F. Volker, J.L. Delgado, Angew. Chem. Int. Ed. 54 (2015) 9757–9759..

[9] H. Mu, F. Hu, R. Wang, J. Jia and S. Xiao, J. Lumin. , 2020, 226, 117493..

[10] X. Z. Deng, Q. Q. Zhao, Y. Q. Zhao, & M. Q. Cai. Theoretical study on photoelectric properties of lead-free mixed inorganic perovskite RbGe1-xSnxI3. Current Applied Physics, 19(3), 279-284 (2019).

[11] A. Bouzaid, Y. Ziat, H. Belkhanchi, H. Hamdani, A. Koufi, M. Miri, ... & Z. Zarhri. Ab initio study of the structural, electronic, and optical properties of MgTiO3 perovskite materials doped with N and P. E3S Web of Conferences. (2024), (Vol. 582, p. 02006). EDP Sciences.

[12] A. Koufi, Y. Ziat, H. Belkhanchi, M. Miri, N. Lakouari ... & F. Z. Baghli. A computational study of the structural and thermal conduct of MgCrH3 and MgFeH3 perovskite-type hydrides: FP-LAPW and BoltzTraP insight. (2024), E3S Web of Conferences (Vol. 582, p. 02003). EDP Sciences. https://doi.org/10.1051/e3sconf/202458202003.

[13] A. S. Bhalla, R. Guo, & R. Roy. The perovskite structure—a review of its role in ceramic science and technology. Materials research innovations, 4(1), 3-26 (2000).

[14] Y. Wang, J. Lv, P. Gao, & Y. Ma. Crystal structure prediction via efficient sampling of the potential energy surface. Accounts of Chemical Research, 55(15), 2068-2076. (2022).

[15] S. Karlheinz. "DFT calculations of solids with LAPW and WIEN2k." Journal of Solid State Chemistry 176.2 (2003): 319-328.

[16] A. Bouzaid, Y. Ziat, & H. Belkhanchi. Prediction the effect of (S, Se, Te) doped MgTiO3 on optoelectronic, catalytic, and pH conduct as promised candidate photovoltaic device: Ab initio framework. International Journal of Hydrogen Energy, (2025), 100, 20-32. https://doi.org/10.1016/j.ijhydene.2024.12.284.

[17] S. Bouhmaidi, R. K. Pingak, A. Azouaoui, A. Harbi, M. Moutaabbid, & L. Setti. Ab initio study of structural, elastic, electronic, optical and thermoelectric properties of cubic Ge-based fluoroperovskites AGeF3 (A= K, Rb and Fr) (2023), Solid State Communications, 369, 115206.

[18] M. S. Alam, M. Saiduzzaman, A. Biswas, T. Ahmed, A. Sultana, & K. M. Hossain. Tuning band gap and enhancing optical functions of AGeF3 (A= K, Rb) under pressure for improved optoelectronic applications. Scientific Reports, 12(1), 8663 (2022).

[19] M. Houari, B. Bouadjemi, S. Haid, M. Matougui, T. Lantri, Z. Aziz, ... & B. Bouhafs. Semiconductor behavior of halide perovskites AGeX 3 (A= K, Rb and Cs; X= F, Cl and

Br): first-principles calculations. Indian Journal of Physics, 94, (2020), 455-467.

[20] M. A. Sarker, M. Muntasir, M. A. Momin, M. Solayman, & M. R. Islam. Pressure-Induced Structural, Electronic, and Optical Properties of Lead-Free NaGeX3 (X= F, Cl, Br, and I) Perovskites: First-Principles Calculation. Advanced Theory (2024), and Simulations, 7(7), 2400112..

[21] J. K. Rony, M. N. Hasan, M. N. Rifat, M. Saiduzzaman, & M. Islam. Pressure-induced DFT evaluation of MSnI3 (M= K, Rb) perovskites for electronic phase transition and enhanced optoelectronic utilization. Computational and Theoretical Chemistry, (2024), 1233, 114512..

[22] M. D. Ratul Hasan, I. A. Apon, I. Ahmed Ovi, & F. T. Zahra. Impact of applied pressure on tin-based cubic halide perovskite ASnX3 (A= Li, Na and X= Cl, Br, and I) in reference to their optoelectronic applications. International Journal (2024), of Energy Research, 2024(1), 8213804.

[23] S. Pooja, P. Ranjan, and T. Chakraborty. "DFT and TD-DFT studies of perovskite materials LiAX3 (A= Ge, Sn; X= F, Cl, Br, I) in reference to their solar cell applications." Materials Today Sustainability 26 (2024): 100791.

[24] N. A. Abdulkareem, B. M. Ilyas, S. A. & Sami. A first principle investigation of the non-synthesized cubic perovskite LiGeX3 (X= I, Br, and Cl). Materials Science in Semiconductor Processing, 131, 105858 (2021).

[25] K. Gesi, K. Ozawa, & S. Hirotsu. Effect of hydrostatic pressure on the structural phase transitions in CsPbCl3 and CsPbBr3. Journal of the Physical Society of Japan, 38(2), 463-466 (1975).

[26] L. Zhang, L. Wang, K. Wang, & B. Zou. Pressure-induced structural evolution and optical properties of metal-halide perovskite CsPbCl3. The Journal of Physical Chemistry C, 122(27), 15220-15225 (2018).

[27] Y. Huang, Z. Li. K. Hu, & X. Shao. First principles investigation on pressure induced phase transition and photocatalytic properties in RbPbCl3. Computational Materials Science, 143, 403-410 (2018).

[28] I. M. Alsalamah, A. Shaari, N. A. Alsaif, S. A. Yamusa, G. Lakshminarayana, & N. Rekik. Exploring the structural properties and the optoelectronic features of RbPbX3 (X= Cl, F) perovskite crystals for solar cells solicitations: (2023)., Showcasing the DFT predictions. Chemical Physics, 573, 111978.

[29] M. R. Hasan, I. A Apon, M. M. Islam, J. Y. Al-Humaidi, & M. R. Islam. First principles calculations to investigate structural, mechanical, electronic, optical and magnetic properties of LiGeX3 (X= Cl, Br, and I) perovskite under (2025),, pressure effect. Materials Science and Engineering: B, 313, 117936..

[30] P. Blaha, K. Schwarz, F. Tran,R. Laskowski,G.K.Madsen,L.D. Marks,WIEN2k: an APW+lo program for calculating the properties of solids, J. Chem. Phys. 152 (2020),074101, https://doi.org/10.1063/1.5143061.

[31] J.P. Perdew, K. Burke, M. Ernzerhof, Generalized gradient approximation made simple. Physical review letters 77 (18) (1996) 3865.

[32] P. Perdew, K. Burke, M. Ernzerhof, Generalized gradient approximation made simple, Phys. Rev. Lett. 77 (1996) 3865, https://doi.org/10.1103/PhysRevLett.77.3865..

[33] R. W. G. Wyckoff, Crystal Structures, 2nd ed., Vol. 1(John Wiley & Sons, (1963)..

[34] Abdulkareem, A. Nawzad M. I. Bahaa, and A. S. Sarkawt. "A first principle investigation of the non-synthesized cubic perovskite LiGeX3 (X= I, Br, and Cl)." Materials Science in Semiconductor Processing 131 (2021): 105858..

[35] T. Katsura, Y. Tange, A simple derivation of the Birch–Murnaghan equations of state (EOSs) and comparison with EOSs derived from other definitions of finite strain, Minerals 9(2019)745, https://doi.org/10.3390/min9120745.

[36] I.N. Frantsevich, F. F. Voronov S.A. Bokuta. Handbook of elastic constants and elastic moduli of metals and nonmetals. Kiev: Naukova Dumka; 1983.

[37] V. G. Tyuterev, & N. Vast. Murnaghan's equation of state for the electronic ground state energy. Computational materials science, 38(2), 350-353. (2006), https://doi.org/10.1016/j.commatsci.2005.08.012.

[38] F. Mouhat F-X. Coudert. Necessary and sufficient elastic stability conditions in various crystal systems. Phys Rev B. 2014;90:224104.

[39] J.Wang and Y. Zhou, Phys. Rev. B 69, 214111 (2004)..

[40] Max Born, On the stability of crystal lattices. I. Mathematical Proceedings of the Cambridge Philosophical Society, 36, pp 160172(1940), DOI:10.1017/S0305004100017138..

[41] Y. O. Ciftci, & M. Evecen. First principle study of structural, electronic, mechanical, dynamic and optical properties of half-Heusler compound LiScSi under pressure. Phase Transit. 91, 1206–1222 (2018)..

[42] F. Herman."Theoretical investigation of the electronic energy band structure of solids." Reviews of Moder 4 Physics 30.1 (1958): 102..

[43] J. Musil, F. Kunc, H. Zeman, H. Polakova, Relationships between hardness, Young's modulus and elastic recovery in hard nanocomposite coatings, Surf. Coating. Technol. 154 (2–3) (2002) 304–313, https://doi.org/10.1016/S0257-8972(01)01714 5.

[44] A.M. Shawahni, M.S. Abu-Jafar, R.T. Jaradat, T. Ouahrani, R. Khenata, A. A. Mousa, K.F. Ilaiwi, Structural, elastic, electronic and optical properties of SrTMO3 (TM= Rh, Zr) compounds: insights from FP-LAPW study, Materials 11 (10) (2018)2057,, https://doi.org/10.3390/ma11102057.

[45] R. Hill, The elastic behaviour of a crystalline aggregate, Proc. Phys. Soc. 65 (5)(1952) 349–354, https://doi.org/10.1088/0370-1298/65/5/307.

[46] A. Reuss, Berechnung der fließgrenze von mischkristallen auf grund der plastizitätsbedingung für einkristalle, Z. Angew. Math. Mech. 9 (1929) 49–58.

[47] S. F. Pugh. XCII. Relations between the elastic moduli and the plastic properties of polycrystalline pure metals. The London, Edinburgh, and Dublin Philosophical Magazine and Journal of Science, 45(367), 823-843. (1954), https://doi.org/10.1080/14786440808520496.

[48] G. Wang, Y. Li. Z. Jiang, X. Chong, & J. Feng. Balance between strength and ductility of dilute Fe2B by high-throughput first-principles calculations. Ceramics International, 47(4), 4758-4768. (2021), https://doi.org/10.1016/j.ceramint.2020.10.045.

[49] H. Bouafia, S. Hiadsi, B. Abidri, A. Akriche, L. Ghalouci, B. Sahli. Structural, elastic, electronic and thermodynamic properties of KTaO3 and NaTaO3: Ab initio investigations. Computational Materials Science, 75(), 1–8. (2013)., doi:10.1016/j.commatsci.2013.03.030.

[50] X. Zhu, S.G. Louie, Quasiparticle band structure of thirteen semiconductors and insulators, Phys. Rev. B 43 (17) (1991) 14142,.

[51] A. P. Nayak, S. Bhattacharyya, J. Zhu, J. Liu, X. Wu, T. Pandey, ... & J. F. Lin. Pressure-induced semiconducting to metallic transition in multilayered molybdenum disulphide. Nature communications, 5(1), 1-9 (2014).

[52] M. Radjai, A. Bouhemadou, D. Maouche, Structural, Elastic, Electronic and Optical,

Properties of the Half-Heusler ScPtSb and YPtSb Compounds under Pressure, 2021 arXiv preprint arXiv:2112.09940.

[53] Gray, L. Harold. "The absorption of penetrating radiation." Proceedings of the Royal Society of London. Series A, Containing Papers of a Mathematical and Physical Character 122.790 (1929): 647-668..

[54] S. Hasegawa."Reflection high-energy electron diffraction."Characterization of Materials, 97 (2012): 1925 1938.